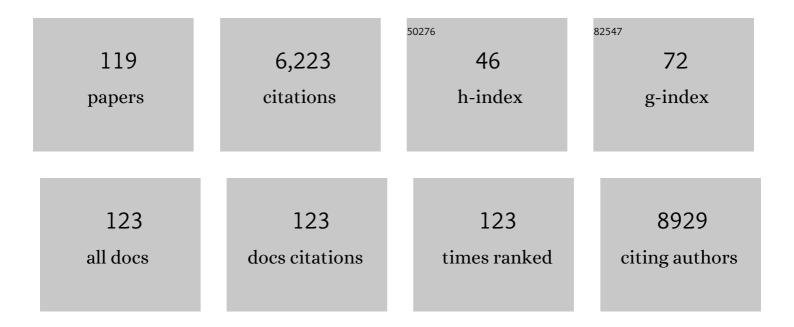
List of Publications by Year in descending order

Source: https://exaly.com/author-pdf/4341706/publications.pdf Version: 2024-02-01



FRIC HANSSEN

#	Article	IF	CITATIONS
1	Extracellular Vesicles Secreted by Glioma Stem Cells Are Involved in Radiation Resistance and Glioma Progression. International Journal of Molecular Sciences, 2022, 23, 2770.	4.1	21
2	Atypical myelinogenesis and reduced axon caliber in the Scn1a variant model of Dravet syndrome: An electron microscopy pilot study of the developing and mature mouse corpus callosum. Brain Research, 2021, 1751, 147157.	2.2	7
3	Plasmon-induced enhancement of ptychographic phase microscopy via sub-surface nanoaperture arrays. Nature Photonics, 2021, 15, 222-229.	31.4	22
4	Novel Virus-Like Particle Vaccine Encoding the Circumsporozoite Protein of Plasmodium falciparum Is Immunogenic and Induces Functional Antibody Responses in Mice. Frontiers in Immunology, 2021, 12, 641421.	4.8	9
5	Characterising the influence of milk fat towards an application for extrusion-based 3D-printing of caseinâ^'whey protein suspensions via the pHâ^'temperature-route. Food Hydrocolloids, 2021, 118, 106642.	10.7	9
6	Design of proteasome inhibitors with oral efficacy in vivo against <i>Plasmodium falciparum</i> and selectivity over the human proteasome. Proceedings of the National Academy of Sciences of the United States of America, 2021, 118, .	7.1	19
7	Structural Characterization of the Type IX Secretion System in Porphyromonas gingivalis. Methods in Molecular Biology, 2021, 2210, 113-121.	0.9	1
8	Colorimetric histology using plasmonically active microscope slides. Nature, 2021, 598, 65-71.	27.8	36
9	Tailoring the structure of casein micelles through a multifactorial approach to manipulate rennet coagulation properties. Food Hydrocolloids, 2020, 101, 105414.	10.7	13
10	Ordered Mesoporous Metal–Phenolic Network Particles. Journal of the American Chemical Society, 2020, 142, 335-341.	13.7	85
11	High frequency acoustic cell stimulation promotes exosome generation regulated by a calcium-dependent mechanism. Communications Biology, 2020, 3, 553.	4.4	65
12	Antibacterial Action of Nanoparticles by Lethal Stretching of Bacterial Cell Membranes. Advanced Materials, 2020, 32, e2005679.	21.0	102
13	Imaging of dairy emulsions <i>via</i> a novel approach of transmission electron cryogenic microscopy using beam exposure. Soft Matter, 2020, 16, 7888-7892.	2.7	4
14	Efficient Transmission Electron Microscopy Characterization of Cell–Nanostructure Interfacial Interactions. Journal of the American Chemical Society, 2020, 142, 15649-15653.	13.7	18
15	The multi-faceted mechano-bactericidal mechanism of nanostructured surfaces. Proceedings of the National Academy of Sciences of the United States of America, 2020, 117, 12598-12605.	7.1	119
16	The structure of the PA28–20S proteasome complex from Plasmodium falciparum and implications for proteostasis. Nature Microbiology, 2019, 4, 1990-2000.	13.3	31
17	Delayed death in the malaria parasite Plasmodium falciparum is caused by disruption of prenylation-dependent intracellular trafficking. PLoS Biology, 2019, 17, e3000376.	5.6	73
18	Thermally coupled dark-anoxia incubation: A platform technology to induce auto-fermentation and thus cell-wall thinning in both nitrogen-replete and nitrogen-deplete Nannochloropsis slurries. Bioresource Technology, 2019, 290, 121769.	9.6	9

#	Article	IF	CITATIONS
19	Interaction of Giant Unilamellar Vesicles with the Surface Nanostructures on Dragonfly Wings. Langmuir, 2019, 35, 2422-2430.	3.5	18
20	Structure and Function of the Proteasome Activator PA28 of the Malaria Parasite Plasmodium falciparum. Microscopy and Microanalysis, 2019, 25, 1324-1325.	0.4	0
21	How Does the Internal Structure of Cardiac Muscle Cells Regulate Cellular Metabolism?. Microscopy and Microanalysis, 2019, 25, 240-241.	0.4	Ο
22	Display of malaria transmission-blocking antigens on chimeric duck hepatitis B virus-derived virus-like particles produced in Hansenula polymorpha. PLoS ONE, 2019, 14, e0221394.	2.5	14
23	A Family of Dual-Activity Glycosyltransferase-Phosphorylases Mediates Mannogen Turnover and Virulence in Leishmania Parasites. Cell Host and Microbe, 2019, 26, 385-399.e9.	11.0	33
24	Identification of Two Independent COL5A1 Variants in Dogs with Ehlers–Danlos Syndrome. Genes, 2019, 10, 731.	2.4	13
25	Analysis of extracellular vesicles generated from monocytes under conditions of lytic cell death. Scientific Reports, 2019, 9, 7538.	3.3	39
26	Towards sustainable microalgal biomass processing: anaerobic induction of autolytic cell-wall self-ingestion in lipid-rich <i>Nannochloropsis</i> slurries. Green Chemistry, 2019, 21, 2967-2982.	9.0	34
27	In Situ Monitoring of Bacteria under Antimicrobial Stress Using 31P Solid-State NMR. International Journal of Molecular Sciences, 2019, 20, 181.	4.1	34
28	Automated segmentation of cardiomyocyte Z-disks from high-throughput scanning electron microscopy data. BMC Medical Informatics and Decision Making, 2019, 19, 272.	3.0	7
29	Multimodal analysis of <i>Plasmodium knowlesi</i> â€infected erythrocytes reveals large invaginations, swelling of the host cell, and rheological defects. Cellular Microbiology, 2019, 21, e13005.	2.1	20
30	A recurrent COL6A1 pseudoexon insertion causes muscular dystrophy and is effectively targeted by splice-correction therapies. JCI Insight, 2019, 4, .	5.0	33
31	The Golgi ribbon in mammalian cells negatively regulates autophagy by modulating mTOR activity. Journal of Cell Science, 2018, 131, .	2.0	44
32	An automated workflow for segmenting single adult cardiac cells from large-volume serial block-face scanning electron microscopy data. Journal of Structural Biology, 2018, 202, 275-285.	2.8	27
33	Sequential Membrane Rupture and Vesiculation during Plasmodium berghei Gametocyte Egress from the Red Blood Cell. Scientific Reports, 2018, 8, 3543.	3.3	24
34	Biochemical transformation of calciprotein particles in uraemia. Bone, 2018, 110, 355-367.	2.9	49
35	Biologically active constituents of the secretome of human W8B2+ cardiac stem cells. Scientific Reports, 2018, 8, 1579.	3.3	26
36	Clickable Cubosomes for Antibody-Free Drug Targeting and Imaging Applications. Bioconjugate Chemistry, 2018, 29, 149-157.	3.6	30

3

#	Article	IF	CITATIONS
37	Automated framework to reconstruct 3D model of cardiac Z-disk: an image processing approach. , 2018, , .		6
38	Insights on the impact of mitochondrial organisation on bioenergetics in high-resolution computational models of cardiac cell architecture. PLoS Computational Biology, 2018, 14, e1006640.	3.2	23
39	Creating a Structurally Realistic Finite Element Geometric Model of a Cardiomyocyte to Study the Role of Cellular Architecture in Cardiomyocyte Systems Biology. Journal of Visualized Experiments, 2018, , .	0.3	3
40	Gel-Mediated Electrospray Assembly of Silica Supraparticles for Sustained Drug Delivery. ACS Applied Materials & Interfaces, 2018, 10, 31019-31031.	8.0	35
41	High Aspect Ratio Nanostructures Kill Bacteria <i>via</i> Storage and Release of Mechanical Energy. ACS Nano, 2018, 12, 6657-6667.	14.6	120
42	Changes in mitochondrial morphology and organization can enhance energy supply from mitochondrial oxidative phosphorylation in diabetic cardiomyopathy. American Journal of Physiology - Cell Physiology, 2017, 312, C190-C197.	4.6	33
43	Mefloquine targets the Plasmodium falciparum 80S ribosome to inhibit protein synthesis. Nature Microbiology, 2017, 2, 17031.	13.3	128
44	A Semi-Automated Workflow for Segmenting Contents of Single Cardiac Cells from Serial-Block-Face Scanning Electron Microscopy Data. Microscopy and Microanalysis, 2017, 23, 240-241.	0.4	4
45	A computational study of the role of mitochondrial organization on cardiac bioenergetics. , 2017, 2017, 2017, 2696-2699.		2
46	A nanomechanical study of the effects of colistin on the Klebsiella pneumoniae AJ218 capsule. European Biophysics Journal, 2017, 46, 351-361.	2.2	12
47	The exported chaperone Hsp70-x supports virulence functions for Plasmodium falciparum blood stage parasites. PLoS ONE, 2017, 12, e0181656.	2.5	45
48	Disrupting assembly of the inner membrane complex blocks Plasmodium falciparum sexual stage development. PLoS Pathogens, 2017, 13, e1006659.	4.7	69
49	Haemoglobin degradation underpins the sensitivity of early ring stage <i>Plasmodium falciparum</i> to artemisinins. Journal of Cell Science, 2016, 129, 406-16.	2.0	78
50	Structural Insights into the PorK and PorN Components of the Porphyromonas gingivalis Type IX Secretion System. PLoS Pathogens, 2016, 12, e1005820.	4.7	67
51	A Third hand for array tomography. Microscopy and Microanalysis, 2016, 22, 1152-1153.	0.4	1
52	Infectivity of Plasmodium falciparum in Malaria-Naive Individuals Is Related to Knob Expression and Cytoadherence of the Parasite. Infection and Immunity, 2016, 84, 2689-2696.	2.2	14
53	Immobilized Particle Imaging for Quantification of Nano- and Microparticles. Langmuir, 2016, 32, 3532-3540.	3.5	14
54	Inhibition of hIAPP Amyloid Aggregation and Pancreatic β-Cell Toxicity by OH-Terminated PAMAM Dendrimer. Small, 2016, 12, 1615-1626.	10.0	99

#	Article	IF	CITATIONS
55	Atomic force microscopy of bacteria reveals the mechanobiology of pore forming peptide action. Biochimica Et Biophysica Acta - Biomembranes, 2016, 1858, 1091-1098.	2.6	42
56	Oncogenic epithelial cell-derived exosomes containing Rac1 and PAK2 induce angiogenesis in recipient endothelial cells. Oncotarget, 2016, 7, 19709-19722.	1.8	56
57	Distinct properties of the egress-related osmiophilic bodies in male and female gametocytes of the rodent malaria parasite <i>Plasmodium berghei</i> . Cellular Microbiology, 2015, 17, 355-368.	2.1	46
58	A repeat sequence domain of the ringâ€exported proteinâ€1 of <scp><i>P</i></scp> <i>lasmodium falciparum</i> controls export machinery architecture and virulence protein trafficking. Molecular Microbiology, 2015, 98, 1101-1114.	2.5	20
59	A molecular nematic liquid crystalline material for high-performance organic photovoltaics. Nature Communications, 2015, 6, 6013.	12.8	541
60	Limisphaera ngatamarikiensis gen. nov., sp. nov., a thermophilic, pink-pigmented coccus isolated from subaqueous mud of a geothermal hotspring. International Journal of Systematic and Evolutionary Microbiology, 2015, 65, 1114-1121.	1.7	20
61	Aberrant Mitochondria in a Bethlem Myopathy Patient with a Homozygous Amino Acid Substitution That Destabilizes the Collagen VI α2(VI) Chain. Journal of Biological Chemistry, 2015, 290, 4272-4281.	3.4	23
62	Interactions between Plasmodium falciparum skeleton-binding protein 1 and the membrane skeleton of malaria-infected red blood cells. Biochimica Et Biophysica Acta - Biomembranes, 2015, 1848, 1619-1628.	2.6	24
63	Thermorudis pharmacophila sp. nov., a novel member of the class Thermomicrobia isolated from geothermal soil, and emended descriptions of Thermomicrobium roseum, Thermomicrobium carboxidum, Thermorudis peleae and Sphaerobacter thermophilus. International Journal of Systematic and Evolutionary Microbiology. 2015. 65. 4479-4487.	1.7	32
64	A Mechanism for Actin Filament Severing by Malaria Parasite Actin Depolymerizing Factor 1 via a Low Affinity Binding Interface. Journal of Biological Chemistry, 2014, 289, 4043-4054.	3.4	22
65	The Apical Complex Provides a Regulated Gateway for Secretion of Invasion Factors in Toxoplasma. PLoS Pathogens, 2014, 10, e1004074.	4.7	92
66	Quantitative analysis of <scp><i>P</i></scp> <i>lasmodium</i> ookinete motion in three dimensions suggests a critical role for cell shape in the biomechanics of malaria parasite gliding motility. Cellular Microbiology, 2014, 16, 734-750.	2.1	45
67	A lysineâ€rich membraneâ€associated PHISTb protein involved in alteration of the cytoadhesive properties of Plasmodium falciparum â€infected red blood cells. FASEB Journal, 2014, 28, 3103-3113.	0.5	46
68	Thermoflavifilum aggregans gen. nov., sp. nov., a thermophilic and slightly halophilic filamentous bacterium from the phylum Bacteroidetes. International Journal of Systematic and Evolutionary Microbiology, 2014, 64, 1264-1270.	1.7	39
69	The role of solvent vapor annealing in highly efficient air-processed small molecule solar cells. Journal of Materials Chemistry A, 2014, 2, 9048.	10.3	133
70	Membrane-Wrapping Contributions to Malaria Parasite Invasion of the Human Erythrocyte. Biophysical Journal, 2014, 107, 43-54.	0.5	85
71	Morphology Change and Improved Efficiency in Organic Photovoltaics via Hexa- <i>peri</i> -hexabenzocoronene Templates. ACS Applied Materials & Interfaces, 2014, 6, 8824-8835.	8.0	17
72	Local regularization of tilt projections reduces artifacts in electron tomography. Journal of Structural Biology, 2014, 186, 28-37.	2.8	8

#	Article	IF	CITATIONS
73	Cryo-EM structure of the Plasmodium falciparum 80S ribosome bound to the anti-protozoan drug emetine. ELife, 2014, 3, .	6.0	274
74	Export of virulence proteins by malaria-infected erythrocytes involves remodeling of host actin cytoskeleton. Blood, 2014, 124, 3459-3468.	1.4	68
75	Electron tomography of <i>Plasmodium falciparum</i> merozoites reveals core cellular events that underpin erythrocyte invasion. Cellular Microbiology, 2013, 15, 1457-1472.	2.1	82
76	Spatial and temporal mapping of the PfEMP1 export pathway in <i>Plasmodium falciparum</i> . Cellular Microbiology, 2013, 15, 1401-1418.	2.1	69
77	Spatial association with PTEX complexes defines regions for effector export into Plasmodium falciparum-infected erythrocytes. Nature Communications, 2013, 4, 1415.	12.8	79
78	2SDP-01 High resolution imaging of malaria parasites with light, x-rays and electrons(2SDP ASB-BSJ) Tj ETQq0 0 Seibutsu Butsuri, 2013, 53, S99.	0 rgBT /Ov 0.1	verlock 10 Tf 0
79	Fetuin-A-Containing Calciprotein Particles Reduce Mineral Stress in the Macrophage. PLoS ONE, 2013, 8, e60904.	2.5	138
80	The Exported Protein PbCP1 Localises to Cleft-Like Structures in the Rodent Malaria Parasite Plasmodium berghei. PLoS ONE, 2013, 8, e61482.	2.5	30
81	Prionâ€infected cells regulate the release of exosomes with distinct ultrastructural features. FASEB Journal, 2012, 26, 4160-4173.	0.5	131
82	Origin, composition, organization and function of the inner membrane complex of <i>Plasmodium falciparum</i> gametocytes. Journal of Cell Science, 2012, 125, 2053-63.	2.0	105
83	Improving the quality of electron tomography image volumes using pre-reconstruction filtering. Journal of Structural Biology, 2012, 180, 132-142.	2.8	16
84	Shape-shifting gametocytes: how and why does P. falciparum go banana-shaped?. Trends in Parasitology, 2012, 28, 471-478.	3.3	48
85	Soft X-ray microscopy analysis of cell volume and hemoglobin content in erythrocytes infected with asexual and sexual stages of Plasmodium falciparum. Journal of Structural Biology, 2012, 177, 224-232.	2.8	139
86	A 95 kDa protein of <i>Plasmodium vivax</i> and <i>P. cynomolgi</i> visualized by threeâ€dimensional tomography in the caveola–vesicle complexes (Schüffner's dots) of infected erythrocytes is a member of the PHIST family. Molecular Microbiology, 2012, 84, 816-831.	2.5	62
87	Cryo transmission X-ray imaging of the malaria parasite, P. falciparum. Journal of Structural Biology, 2011, 173, 161-168.	2.8	58
88	Relevant Assay to Study the Adhesion of Plasmodium falciparum-Infected Erythrocytes to the Placental Epithelium. PLoS ONE, 2011, 6, e21126.	2.5	8
89	Genetic ablation of a Maurer's cleft protein prevents assembly of the <i>Plasmodium falciparum</i> virulence complex. Molecular Microbiology, 2011, 81, 982-993.	2.5	37

90 Super-resolution optical imaging of malaria parasites. , 2011, , .

#	Article	IF	CITATIONS
91	Minimal requirements for actin filament disassembly revealed by structural analysis of malaria parasite actin-depolymerizing factor 1. Proceedings of the National Academy of Sciences of the United States of America, 2011, 108, 9869-9874.	7.1	43
92	Tracking Glideosome-Associated Protein 50 Reveals the Development and Organization of the Inner Membrane Complex of Plasmodium falciparum. Eukaryotic Cell, 2011, 10, 556-564.	3.4	51
93	Whole cell imaging reveals novel modular features of the exomembrane system of the malaria parasite, Plasmodium falciparum. International Journal for Parasitology, 2010, 40, 123-134.	3.1	76
94	Cellular architecture of Plasmodium falciparum-infected erythrocytes. International Journal for Parasitology, 2010, 40, 1127-1135.	3.1	49
95	MAHRP2, an exported protein of Plasmodium falciparum, is an essential component of Maurer's cleft tethers. Molecular Microbiology, 2010, 77, 1136-1152.	2.5	64
96	Digestive-vacuole genesis and endocytic processes in the early intraerythrocytic stages of <i>Plasmodium falciparum</i> . Journal of Cell Science, 2010, 123, 441-450.	2.0	160
97	Hematinâ^'Hematin Self-Association States Involved in the Formation and Reactivity of the Malaria Parasite Pigment, Hemozoin. Biochemistry, 2010, 49, 6804-6811.	2.5	57
98	Ultrastructure of the Asexual Blood Stages of Plasmodium falciparum. Methods in Cell Biology, 2010, 96, 93-116.	1.1	20
99	Characterisation of PfRON6, a Plasmodium falciparum rhoptry neck protein with a novel cysteine-rich domain. International Journal for Parasitology, 2009, 39, 683-692.	3.1	22
100	Whole Cell Imaging of Plasmodium Falciparum Blood Stages. Microscopy and Microanalysis, 2009, 15, 866-867.	0.4	0
101	Functional alteration of red blood cells by a megadalton protein of Plasmodium falciparum. Blood, 2009, 113, 919-928.	1.4	72
102	Electron tomography of the Maurer's cleft organelles of <i>Plasmodium falciparum</i> â€infected erythrocytes reveals novel structural features. Molecular Microbiology, 2008, 67, 703-718.	2.5	80
103	The Twists and Turns of Maurer's Cleft Trafficking in <i>P. falciparum</i> â€Infected Erythrocytes. Traffic, 2008, 9, 187-197.	2.7	64
104	Highâ€resolution Xâ€ray imaging of <i>Plasmodium falciparum</i> â€infected red blood cells. Cytometry Part A: the Journal of the International Society for Analytical Cytology, 2008, 73A, 949-957.	1.5	49
105	The Maurer's cleft protein MAHRP1 is essential for trafficking of PfEMP1 to the surface of <i>Plasmodium falciparum</i> â€infected erythrocytes. Molecular Microbiology, 2008, 68, 1300-1314.	2.5	94
106	Targeted mutagenesis of the ringâ€exported proteinâ€1 of <i>Plasmodium falciparum</i> disrupts the architecture of Maurer's cleft organelles. Molecular Microbiology, 2008, 69, 938-953.	2.5	65
107	A 3D view of the host cell compartment in P.Âfalciparum-infected erythrocytes. Transfusion Clinique Et Biologique, 2008, 15, 72-81.	0.4	15
108	Quantitative phase measurement in coherent diffraction imaging. Optics Express, 2008, 16, 3342.	3.4	21

ERIC HANSSEN

#	Article	IF	CITATIONS
109	Artemisinin and a Series of Novel Endoperoxide Antimalarials Exert Early Effects on Digestive Vacuole Morphology. Antimicrobial Agents and Chemotherapy, 2008, 52, 98-109.	3.2	112
110	Selective permeabilization of the host cell membrane of Plasmodium falciparum-infected red blood cells with streptolysin O and equinatoxin II. Biochemical Journal, 2007, 403, 167-175.	3.7	93
111	LTBP-2 specifically interacts with the amino-terminal region of fibrillin-1 and competes with LTBP-1 for binding to this microfibrillar protein. Matrix Biology, 2007, 26, 213-223.	3.6	116
112	X-ray ultramicroscopy using integrated sample cells. Optics Express, 2006, 14, 7889.	3.4	5
113	βig-h3 Interacts Directly with Biglycan and Decorin, Promotes Collagen VI Aggregation, and Participates in Ternary Complexing with These Macromolecules. Journal of Biological Chemistry, 2006, 281, 7816-7824.	3.4	78
114	MAGP-2 Has Multiple Binding Regions on Fibrillins and Has Covalent Periodic Association with Fibrillin-containing Microfibrils. Journal of Biological Chemistry, 2004, 279, 29185-29194.	3.4	42
115	Covalent and Non-covalent Interactions of \hat{l}^2 ig-h3 with Collagen VI. Journal of Biological Chemistry, 2003, 278, 24334-24341.	3.4	67
116	Molecular Interactions of Biglycan and Decorin with Elastic Fiber Components. Journal of Biological Chemistry, 2002, 277, 3950-3957.	3.4	144
117	Synthesis and structural organization of zonular fibers during development and aging. Matrix Biology, 2001, 20, 77-85.	3.6	35
118	Atomic force microscopy and modeling of natural elastic fibrillin polymers. Biology of the Cell, 1998, 90, 223-228.	2.0	23
119	Purification of Fibrillin-Containing Microfibrils and Collagen VI Microfibrils by Density Gradient Centrifugation. Analytical Biochemistry, 1998, 255, 108-112.	2.4	24